

Synthesis and Characterization of Nanoporous Gold Nanowires

Chunxin Ji and Peter C. Searson*

Department of Materials Science and Engineering, Johns Hopkins University,
Baltimore, Maryland 21218

Received: October 14, 2002

We report on a two-step process for the fabrication of nanoporous nanowires. The fabrication process involves electrochemical deposition of a single-phase binary alloy into a nanoporous template, followed by subsequent etching of the less noble component. These particles are characterized by diameters of 20 nm or larger, lengths of up to tens of microns, and a porous structure with controlled pore dimensions. In contrast to conventional solid nanoparticles, nanoporous nanowires have a high surface area and a well-defined pore morphology. Furthermore, nanoporous segments can be incorporated into multisegment nanorods or nanowires. Here, we demonstrate the fabrication of nanoporous gold (NPG) nanowires and multisegment nanowires incorporating Au/NPG layers and Pt/NPG layers.

Introduction

Solid metallic nanoparticles have been exploited for a wide range of applications that take advantage of their high surface-to-volume ratio.^{1–4} Recently, there has been increasing interest in the anisotropic properties of nanorods and nanowires.^{5–9} Here, we report on the fabrication of nanoporous nanowires. These particles are characterized by diameters of 20 nm or larger, lengths of up to tens of microns, and a porous structure with controlled pore dimensions. In contrast to conventional solid nanoparticles, nanoporous nanowires have a high surface area and a well-defined pore morphology. Furthermore, nanoporous segments can be incorporated into multisegment nanowires.

Nanoporous structures are formed when a single-phase binary alloy containing a noble metal is etched in a suitable solution. Preferential dissolution of the less noble component of the alloy results in the formation of a porous structure of the more noble element. This effect was first reported in the 1920s and has subsequently been observed in Cu–Zn, Au–Cu (ref 10 and references therein), and Au–Ag^{11–14} alloys. The evolution of the porous structure during the dealloying process involves etching of the less noble metal coupled with coarsening of the more noble metal by surface diffusion.^{10,11,14–19}

The Au–Ag system is of interest because Au and Ag both have face-centered-cubic structures with similar lattice parameters and exhibit solid solubility across the entire composition range. Porous Au films have been prepared by dealloying Au_xAg_{1–x} alloys with Au concentrations in the range of 15–35 atom %.^{11–14} Au_xAg_{1–x} alloys have been prepared by casting,^{13,14} thermal evaporation, or sputter deposition.¹⁵ To our knowledge, there have been no reports of the dealloying of electrodeposited Au_xAg_{1–x} alloys. Various solutions have been developed for the electrodeposition of silver^{20–22} and gold,^{23–29} and it is known that both gold and silver can be deposited from basic cyanide solutions.^{22–26}

In this paper, we describe a two-step process for the fabrication of nanoporous nanowires. In the first step, a single-

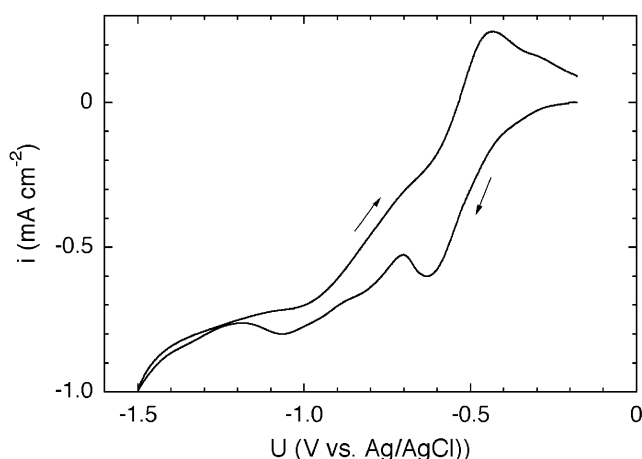


Figure 1. Cyclic voltammograms for 10 mM KAg(CN)₂, 10 mM KAu(CN)₂, and 0.25 M Na₂CO₃ (pH 13) on gold at a scan rate of 10 mV s⁻¹.

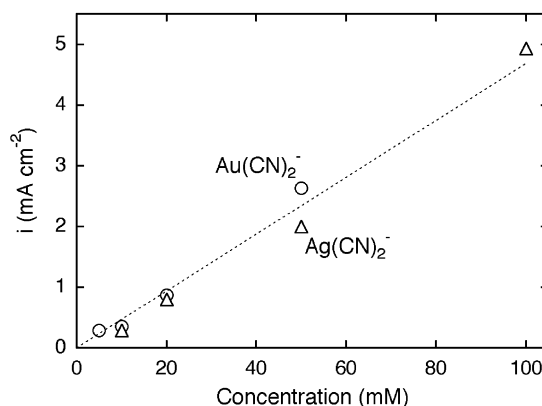


Figure 2. Steady-state deposition currents for gold (○) and silver (Δ) at -1.2 V versus Au(CN)₂⁻ or Ag(CN)₂⁻ concentration. Gold was deposited from a solution containing KAu(CN)₂ and 0.25 M Na₂CO₃ (pH 13), and silver was deposited from a solution containing KAg(CN)₂ and 0.25 M Na₂CO₃ (pH 13).

* To whom correspondence should be addressed. E-mail: searson@jhu.edu.

phase, binary alloy is electrochemically deposited into a nanoporous template.^{30–32} In the second step, the solid nano-

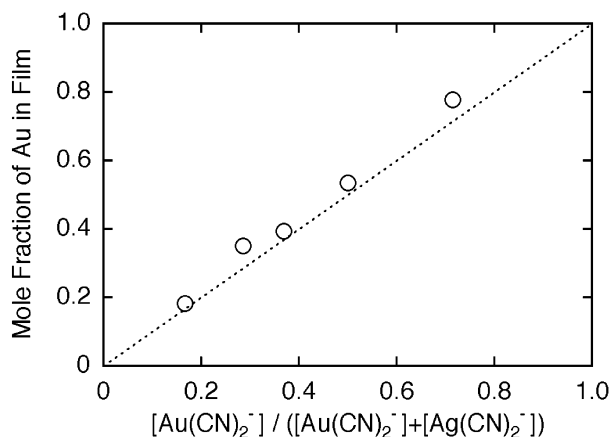


Figure 3. Mole fraction of gold in $\text{Au}_x\text{Ag}_{1-x}$ alloy films deposited at -1.2 V versus the mole fraction of $\text{Au}(\text{CN})_2^-$ in solution. In all cases the thickness of the films was about $3\ \mu\text{m}$. The composition of the films was determined from the XPS Au $4f^7$ and Ag $3d^5$ peaks after sputter cleaning of the surface.

wires are removed from the template, and one component is chemically etched from the alloy. For example, an A_xB_{1-x} alloy is deposited into a porous template, and component B is then chemically etched from the solid nanowires. As long as the concentration of B in the alloy is in the range, e.g., 65–85 atom % Ag for $\text{Au}_x\text{Ag}_{1-x}$ alloys ($0.15 \leq x \leq 0.35$), nanoporous nanowires of component A are formed. The pore structure and surface area are dependent on the concentration of component B and any subsequent annealing treatment.¹³

Experimental Section

$\text{Au}_x\text{Ag}_{1-x}$ alloy thin films were electrodeposited from solutions containing $\text{KAg}(\text{CN})_2$ (99.9%, Alfa Aesar), $\text{KAu}(\text{CN})_2$ (99.99%, Alfa Aesar), and $0.25\ \text{M}\ \text{Na}_2\text{CO}_3$ (99.5%, ACS grade) at pH 13. Thin films were deposited onto gold or silver evaporated onto Si(100) wafers. Prior to deposition, the substrates were sequentially cleaned with acetone, methanol, and deionized distilled H_2O . Experiments were performed in a three-electrode cell with a platinum mesh counter electrode and a Ag/AgCl (3 M NaCl) reference electrode ($U_{\text{eq}} = 0.2\ \text{V}$ vs SHE) positioned close to the substrate surface using a Luggin capillary.

X-ray photoelectron spectra were recorded with a Perkin-Elmer X-ray photoelectron spectrometer using Mg $\text{K}\alpha$ as the X-ray source. The Au $4f^7$ and Ag $3d^5$ peaks were used to determine the relative concentrations of Au and Ag in the films. Scanning electron microscopy (SEM) images were obtained with a JEOL JSM-6700 field emission SEM instrument.

$\text{Au}_x\text{Ag}_{1-x}$ alloy nanowires were fabricated by electrodeposition^{30–32} into Al_2O_3 membranes (Anodisc, Whatman) with a specified pore diameter of 100 nm. We note that the pores are 100 nm in diameter only for a distance of about $1\ \mu\text{m}$ from the back side of the membrane; for the rest of the thickness, the diameter is 200–350 nm.³³ A copper film, evaporated onto the back side of the Al_2O_3 membrane, served as the working electrode.

The $\text{Au}_x\text{Ag}_{1-x}$ alloy nanowires were deposited from a solution containing 100 mM $\text{KAg}(\text{CN})_2$, 20 mM $\text{KAu}(\text{CN})_2$, and $0.25\ \text{M}\ \text{Na}_2\text{CO}_3$ (pH 13) or from a solution containing 50 mM $\text{KAg}(\text{CN})_2$, 20 mM $\text{KAu}(\text{CN})_2$, and $0.25\ \text{M}\ \text{Na}_2\text{CO}_3$ (pH 13).

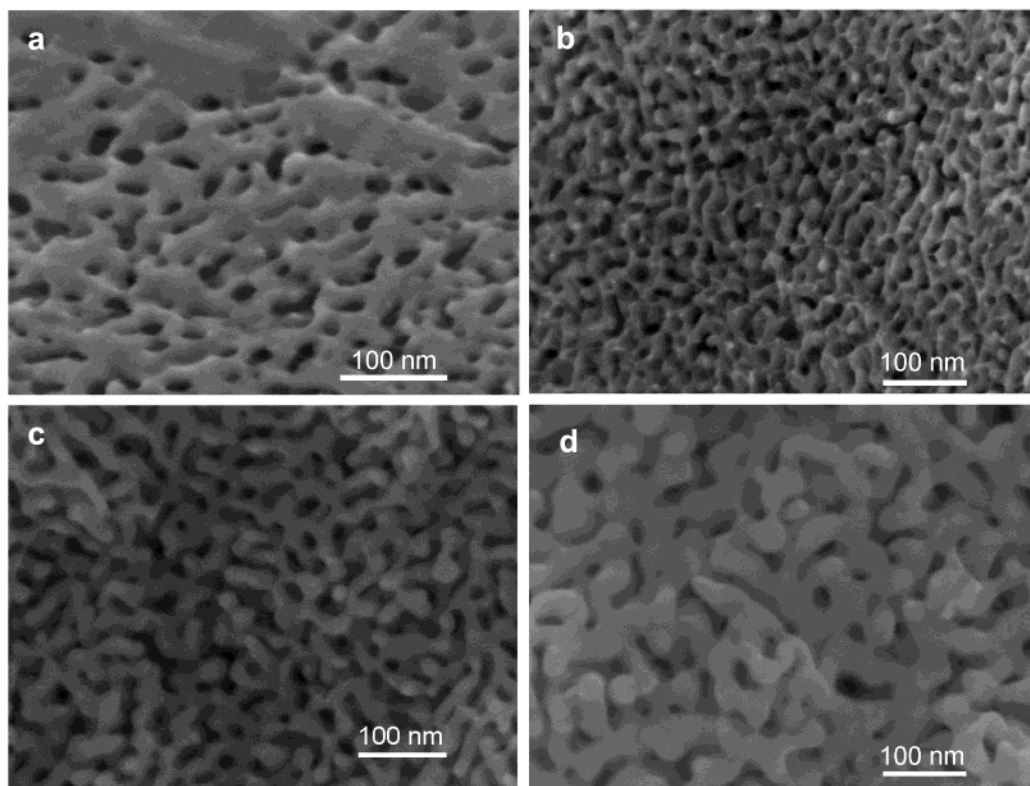


Figure 4. Plan-view SEM images of $\text{Au}_x\text{Ag}_{1-x}$ alloy films after etching in concentrated nitric acid. The films were deposited at -1.2 V on Au. (a) Etched $\text{Au}_{0.40}\text{Ag}_{0.60}$ film deposited from a solution containing 60 mM $\text{KAg}(\text{CN})_2$, 35 mM $\text{KAu}(\text{CN})_2$, and $0.25\ \text{M}\ \text{Na}_2\text{CO}_3$ (pH 13), (b) etched $\text{Au}_{0.32}\text{Ag}_{0.68}$ film deposited from a solution containing 50 mM $\text{KAg}(\text{CN})_2$, 20 mM $\text{KAu}(\text{CN})_2$, and $0.25\ \text{M}\ \text{Na}_2\text{CO}_3$ (pH 13), (c) etched $\text{Au}_{0.26}\text{Ag}_{0.74}$ film deposited from a solution containing 100 mM $\text{KAg}(\text{CN})_2$, 30 mM $\text{KAu}(\text{CN})_2$, and $0.25\ \text{M}\ \text{Na}_2\text{CO}_3$ (pH 13), and (d) etched $\text{Au}_{0.18}\text{Ag}_{0.82}$ film deposited from a solution containing 100 mM $\text{KAg}(\text{CN})_2$, 20 mM $\text{KAu}(\text{CN})_2$, and $0.25\ \text{M}\ \text{Na}_2\text{CO}_3$ (pH 13). The thickness of the as-deposited films was about $3\ \mu\text{m}$.

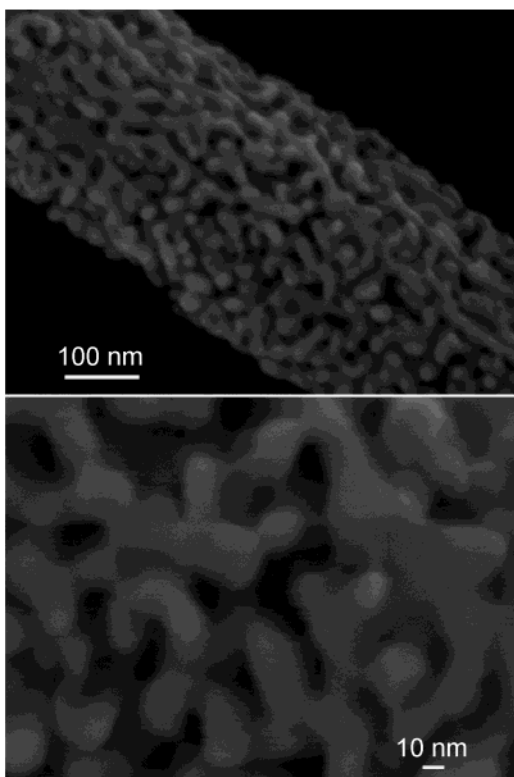


Figure 5. SEM images of NPG nanowires prepared by the etching of $\text{Au}_{0.18}\text{Ag}_{0.82}$ alloy nanowires deposited in an Al_2O_3 template at -1.2 V from a solution containing 100 mM $\text{KAg}(\text{CN})_2$, 20 mM $\text{KAu}(\text{CN})_2$, and 0.25 M Na_2CO_3 (pH 13). The nanowires were removed from the template and etched in concentrated nitric acid.

at -1.2 V (vs Ag/AgCl). Pure gold was deposited from a solution containing 20 mM $\text{KAu}(\text{CN})_2$ and 0.25 M Na_2CO_3 (pH 13) at -1.2 V (vs Ag/AgCl). Pure platinum was deposited from a solution containing 0.0167 M ammonium hexachloroplatinate $[(\text{NH}_4)_2\text{PtCl}_6]$; 44% Pt, Alfa Aesar] and 0.409 M sodium hydrogen phosphate (Na_2HPO_4 ; 98%, Alfa Aesar) (pH 8) at -1.0 V (vs Ag/AgCl).³⁴

The nanowires were stripped from the templates in the following way: The evaporated copper film was dissolved using 0.5 M CuCl_2 and 1 M HCl , and the alumina template was then dissolved in 2 M KOH . The nanowires were cleaned by sequential ultrasonication, centrifugation, and rinsing with deionized distilled water. The nanowires were then transferred and stored in ethanol. Nanoporous gold (NPG) nanowires were prepared by etching of the $\text{Au}_x\text{Ag}_{1-x}$ alloy nanowires in concentrated nitric acid.

The surface area of the nanoporous gold nanowires was determined from BET measurements (Coulter SA3100) using nitrogen adsorption. The $\text{Au}_x\text{Ag}_{1-x}$ alloy nanowires were etched with concentrated nitric acid, and samples of at least 100 mg of the NPG nanowires were used for each BET measurement. Before measurement of the surface area, the samples were annealed at temperatures between 50 and 300 °C for 1 h at a pressure of about 2×10^{-5} Torr.

Results and Discussion

Figure 1 shows a current–voltage curve for the deposition of $\text{Au}_x\text{Ag}_{1-x}$ from a solution containing 10 mM $\text{KAg}(\text{CN})_2$, 10 mM $\text{KAu}(\text{CN})_2$, and 0.25 M Na_2CO_3 (pH 13). The deposition peaks at about -0.6 and -1.05 V correspond to the deposition peaks for silver and gold, respectively.³⁵ On the reverse scan, a diffusion-limited deposition current of about 0.8 mA cm^{-2} is

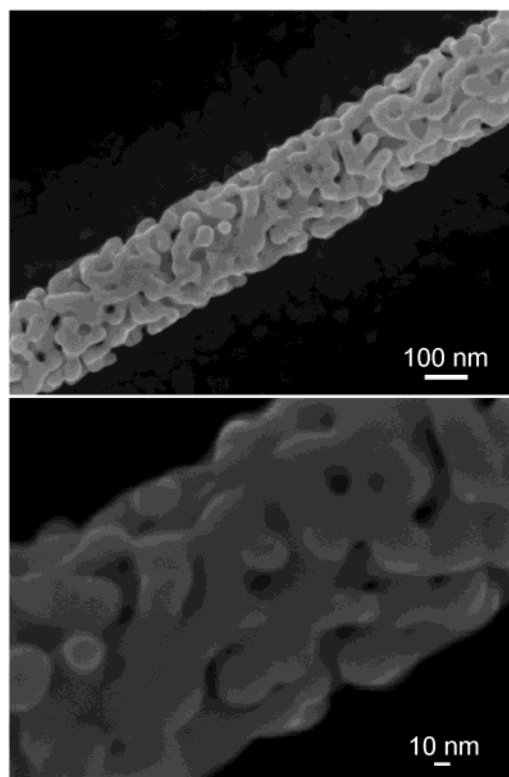


Figure 6. SEM images of an NPG nanowire prepared by the etching of $\text{Au}_{0.32}\text{Ag}_{0.68}$ alloy nanowires deposited at -1.2 V from a solution containing 50 mM $\text{KAg}(\text{CN})_2$, 20 mM $\text{KAu}(\text{CN})_2$, and 0.25 M Na_2CO_3 (pH 13). The nanowires were removed from the template and etched in concentrated nitric acid.

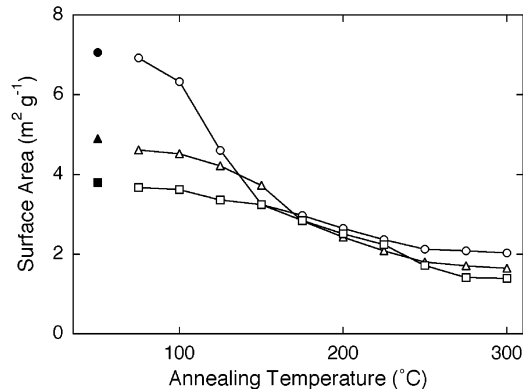


Figure 7. Specific surface area of NPG nanowires versus annealing temperature. The NPG nanowires were obtained by the etching of (○) $\text{Au}_{0.18}\text{Ag}_{0.82}$ alloy nanowires; (△) $\text{Au}_{0.26}\text{Ag}_{0.74}$ alloy nanowires; and (□) $\text{Au}_{0.32}\text{Ag}_{0.68}$ alloy nanowires. The solid symbols correspond to the unannealed NPG nanowires.

observed up to about -1.0 V. At more positive potentials, a peak is seen at about -0.45 V due to the stripping of silver.

Figure 2 shows the steady-state deposition current for pure gold from $\text{Au}(\text{CN})_2^-$ solution and for pure silver from $\text{Ag}(\text{CN})_2^-$ solution at -1.2 V. At this potential, the deposition currents for gold and silver both increase linearly with concentration, indicating that the deposition process is diffusion-limited for both elements.^{35–39} The slopes of the two curves are essentially the same, consistent with the fact that the diffusion coefficients for $\text{Ag}(\text{CN})_2^-$ and $\text{Au}(\text{CN})_2^-$ are both about $1.6 \times 10^{-5} \text{ cm}^2 \text{ s}^{-1}$.^{39–41}

The composition of $\text{Au}_x\text{Ag}_{1-x}$ alloy films deposited at -1.2 V, where the deposition currents for both elements are diffusion-limited, is dependent on the concentrations of $\text{Ag}(\text{CN})_2^-$ and

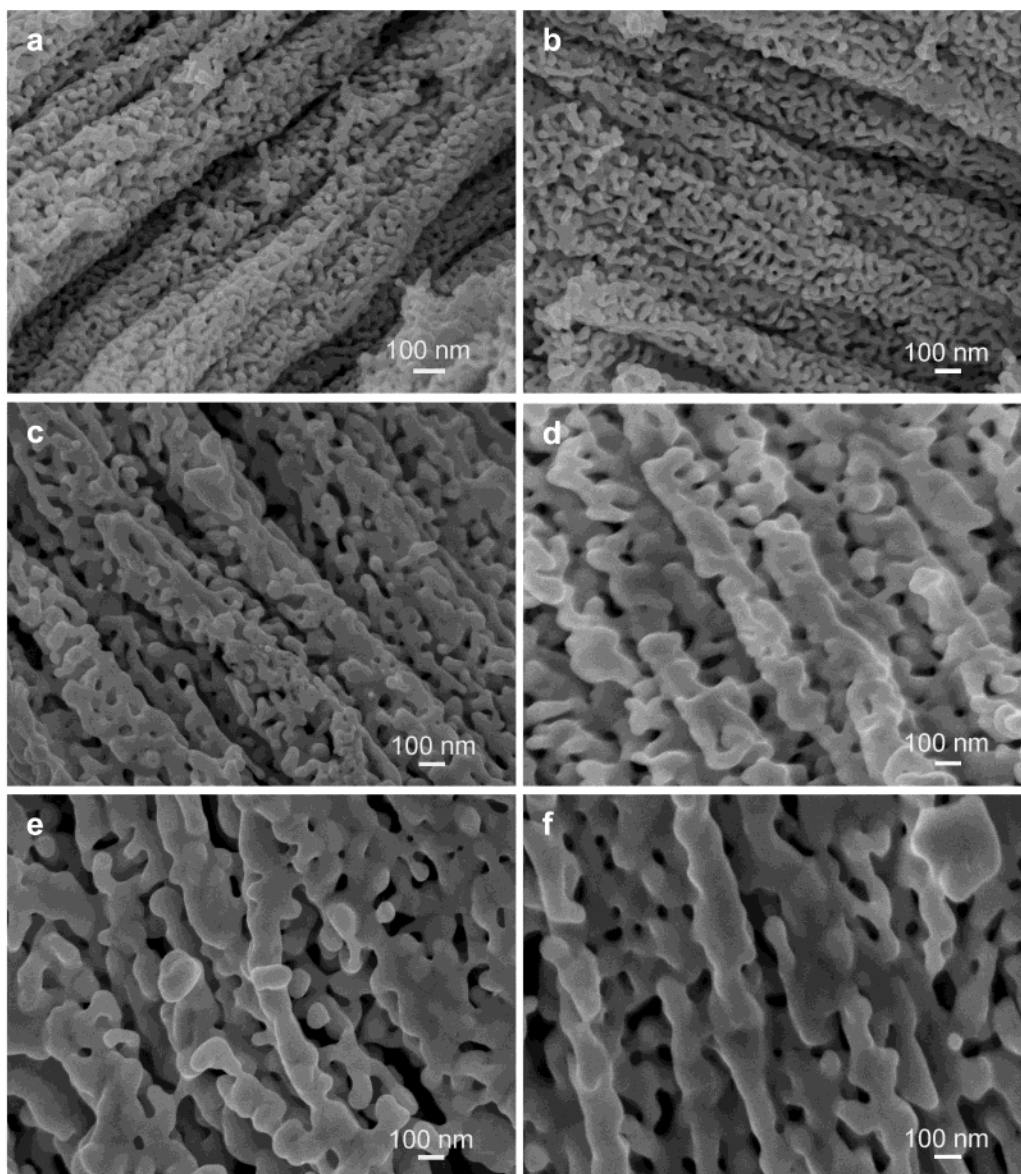


Figure 8. SEM images of NPG nanowires annealed for 1 h at (a) 50, (b) 100, (c) 150, (d) 200, (e) 250, and (f) 300 °C. The nanowires were synthesized by the etching of $\text{Au}_{0.18}\text{Ag}_{0.82}$ alloy nanowires deposited at -1.2 V from a solution containing 100 mM $\text{KAg}(\text{CN})_2$, 20 mM $\text{KAu}(\text{CN})_2$, and 0.25 M Na_2CO_3 (pH 13).

$\text{Au}(\text{CN})_2^-$ in solution. Figure 3 shows the mole fraction of Au in the alloy films versus the fraction of $\text{Au}(\text{CN})_2^-$ in solution determined from the ratio $[\text{Au}(\text{CN})_2^-]/([\text{Ag}(\text{CN})_2^-] + [\text{Au}(\text{CN})_2^-])$. The linear relationship with a slope close to 1.0 illustrates that $\text{Au}_x\text{Ag}_{1-x}$ is an ideal binary alloy system where the ratio of the diffusion-limited deposition currents at any potential and concentration is equal to the composition ratio in the film. The small deviation from ideal behavior is due to the difference in deposition efficiencies: the deposition efficiency for gold films at this potential is 0.78, whereas the deposition efficiency for silver films is 0.75.

Figure 4 shows plan-view SEM images of a series of NPG films prepared by the etching of electrodeposited $\text{Au}_x\text{Ag}_{1-x}$ films with $0.18 \leq x \leq 0.40$. The $\text{Au}_x\text{Ag}_{1-x}$ films were deposited at -1.2 V from solutions with different $\text{Au}(\text{CN})_2^-/\text{Ag}(\text{CN})_2^-$ ratios. For $x = 0.40$ (Figure 4a), the dealloyed film exhibits sparsely distributed nanopores that are 10–30 nm in diameter. For $x = 0.32$, a continuous porous network is formed with a characteristic ligament size of about 10–20 nm. With decreasing mole fraction of gold, the ligament size increased to 20–30

nm for $x = 0.26$ and to 30–40 nm for $x = 0.18$. Similar results have been reported for the dealloying of $\text{Au}_x\text{Ag}_{1-x}$ films deposited by vapor deposition.^{11–14} For films with $x > 0.40$, there is no significant change in surface morphology before and after etching. Cross-sectional SEM images revealed a continuous porous network across the entire thickness of the film for porous Au layers formed by the etching of alloys with $x \leq 0.32$.

NPG nanowires were fabricated by removing $\text{Au}_x\text{Ag}_{1-x}$ alloy nanowires from the alumina template and etching the silver in nitric acid. Figure 5 shows SEM images of NPG nanowires fabricated by etching $\text{Au}_{0.18}\text{Ag}_{0.82}$ alloy nanowires. The NPG nanowires exhibit a porous structure with a ligament size of about 20–30 nm and a pore size of about 20–30 nm.

The morphology of the nanowires is dependent on the alloy composition. Figure 6 shows SEM images of NPG nanowires fabricated by the etching of $\text{Au}_{0.32}\text{Ag}_{0.68}$ alloy nanowires. In this case, the ligament size is about 35–50 nm, and the pore size about 10–40 nm. The increase in ligament size with increasing gold concentration in the $\text{Au}_x\text{Ag}_{1-x}$ alloy is opposite to the dependence seen in thin films^{11–14} (see Figure 4) and is

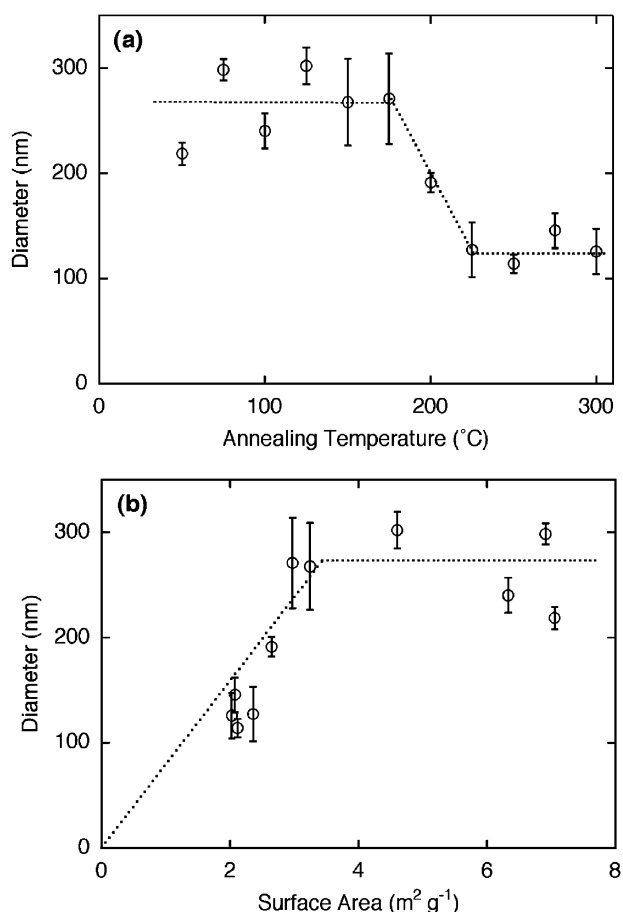


Figure 9. Diameter of the NPG nanowires obtained from SEM images in Figure 8 versus (a) annealing temperature and (b) surface area.

related to coarsening in the cylindrical geometry. These images illustrate that the porosity and morphology of the NPG nanowires can be controlled by varying the composition of the $\text{Au}_x\text{Ag}_{1-x}$ alloy.

The surface area of the NPG nanowires was determined by gas adsorption measurements. Figure 7 shows the specific surface area versus annealing temperature for NPG nanowires. For the unannealed nanowires, the surface area increased with decreasing atomic fraction of gold in the $\text{Au}_x\text{Ag}_{1-x}$ alloy. The surface area was $6.9 \text{ m}^2 \text{ g}^{-1}$ for NPG nanowires synthesized by dealloying $\text{Au}_{0.18}\text{Ag}_{0.82}$ and $3.7 \text{ m}^2 \text{ g}^{-1}$ for NPG nanowires synthesized by dealloying $\text{Au}_{0.32}\text{Ag}_{0.68}$. Annealing the nanowires at temperatures above 50°C results in a decrease in the specific surface area due to coarsening.¹³ With increasing annealing temperature, the specific surface area decreases rapidly and reaches a constant value of $2.0 \text{ m}^2 \text{ g}^{-1}$ for $x = 0.18$ and $1.3 \text{ m}^2 \text{ g}^{-1}$ for $x = 0.32$.

The influence of annealing on the morphology of the NPG nanowires can be seen in the SEM images shown in Figure 8 for NPG nanowires synthesized by the etching of $\text{Au}_{0.18}\text{Ag}_{0.82}$. The images show that the NPG nanowires coarsen with increasing annealing temperature, resulting in a decrease in the porosity. Sintering between nanowires can be seen when the annealing temperature is higher than 175°C . After annealing at 300°C , the nanowires are almost solid cylinders, consistent with surface area measurements shown in Figure 8. Note that the diameter of the NPG nanowires after annealing at 300°C is larger for nanowires fabricated from $\text{Au}_x\text{Ag}_{1-x}$ alloys with higher gold contents (larger x). Thus, the surface area after annealing at 300°C is higher for NPG nanowires fabricated

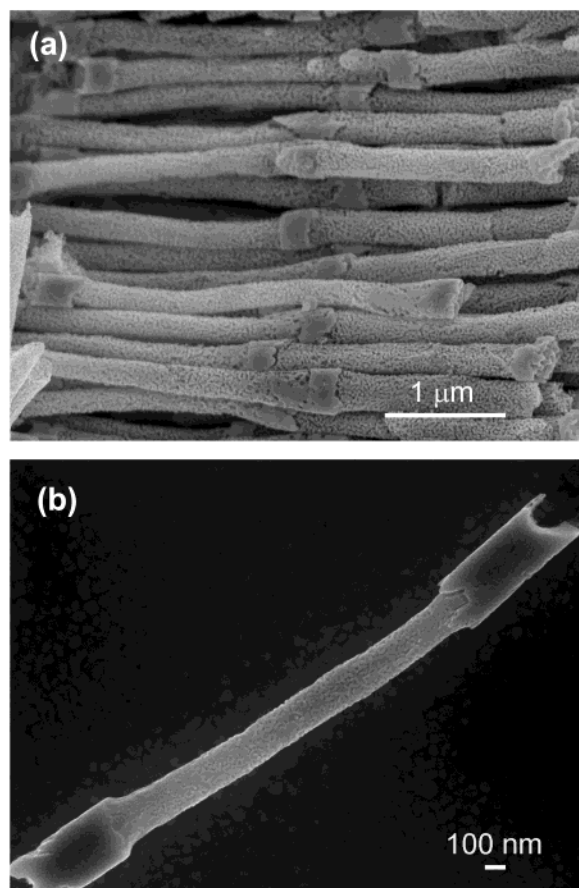


Figure 10. SEM images of multicomponent nanowires. (a) Nanowires with NPG and solid Au and segments fabricated by the etching of $(\text{Au}_{0.18}\text{Ag}_{0.82}/\text{Au})_n$ nanowires. (b) Nanowires with NPG and solid Pt segments fabricated by the etching of $\text{Pt}/\text{Au}_{0.18}\text{Ag}_{0.82}/\text{Pt}$ nanowires.

from $\text{Au}_{0.18}\text{Ag}_{0.82}$ alloys than for those fabricated from $\text{Au}_{0.32}\text{Ag}_{0.68}$ alloys.

Figure 9 displays a plot of the diameter of the NPG nanowires, obtained from the SEM images shown in Figure 8, as a function of annealing temperature and surface area. From Figure 9a, it can be seen that for annealing temperatures below about 150°C , the diameter remains constant with increasing annealing temperatures whereas the specific surface area decreases from 6.9 to $4 \text{ m}^2 \text{ g}^{-1}$, as shown in Figure 7. In this temperature range, the decrease in surface area is due to coarsening. For annealing temperatures above 150°C , the diameter decreases dramatically from 275 to 125 nm , as can be seen in Figure 9b, and the surface area decreases accordingly. The decrease in wire diameter with annealing above 150°C is associated with the onset of sintering.

Nanoporous segments can be incorporated into multisegment nanorods or nanowires. Figure 10a shows an SEM image of a bundle of multisegment nanowires with alternating NPG and solid Au segments formed by the etching of $(\text{Au}_{0.18}\text{Ag}_{0.82}/\text{Au})_2$ nanowires in nitric acid. The $\text{Au}_{0.18}\text{Ag}_{0.82}$ segments were deposited from a solution containing $100 \text{ mM Ag}(\text{CN})_2^-$ and $20 \text{ mM Au}(\text{CN})_2^-$ at -1.2 V , and the Au segments were deposited at -1.2 V from a $20 \text{ mM Au}(\text{CN})_2^-$ solution. The multisegment nanowires are reasonably robust, although a small number of the gold end segments have become detached during ultrasonication and centrifugation. Figure 10b shows multisegment nanowires with a central NPG segment and solid platinum segments at each end. The nanowires were prepared by the etching of $\text{Pt}/\text{Au}_{0.18}\text{Ag}_{0.82}/\text{Pt}$ nanowires. The $\text{Au}_{0.18}\text{Ag}_{0.82}$ segment was deposited from a solution containing 100 mM

$\text{Ag}(\text{CN})_2^-$ and 20 mM $\text{Au}(\text{CN})_2^-$ at -1.2 V. Before etching, the diameter of the $\text{Pt}/\text{Au}_{0.18}\text{Ag}_{0.82}/\text{Pt}$ nanowire was about 320 nm. After etching, the diameter of the NPG segment decreased to about 200 nm, and from the original composition, we obtained a porosity of 53% for NPG nanowires fabricated by the etching of $\text{Au}_{0.18}\text{Ag}_{0.82}$ alloys. The $\text{Pt}/\text{NPG}/\text{Pt}$ nanowires were very robust, with no evidence of segments becoming detached.

Conclusions

Nanoporous gold nanowires have been fabricated by dealloying $\text{Au}_x\text{Ag}_{1-x}$ alloy nanowires ($x = 0.18-0.32$) deposited in Al_2O_3 membranes from a solution containing $\text{KAg}(\text{CN})_2$, $\text{KAu}(\text{CN})_2$, and Na_2CO_3 (pH 13). The NPG nanowires show surface areas as high as $6.9 \text{ m}^2 \text{ g}^{-1}$. The porous structure and surface morphology of the porous nanowires are dependent on the composition of the $\text{Au}_x\text{Ag}_{1-x}$ alloy and on subsequent thermal annealing. Multisegment nanowires containing NPG segments can be obtained by switching solutions during deposition. This technique can be extended to other binary alloy systems for the synthesis of porous metallic nanowires.

Acknowledgment. This work was supported by the JHU MRSEC (DMR-0080031) and the David and Lucile Packard Foundation (Grant 2001-17715). X-ray photoelectron spectroscopy was performed in the JHU/MRSEC-supported Surface Analysis Laboratory.

References and Notes

- Freeman, R. G.; Grabar, K. C.; Allison, K. J.; Bright, R. M.; Davis, J. A.; Guthrie, A. P.; Hommer, M. B.; Jackson, M. A.; Smith, P. C.; Walter, D. G.; Natan, M. J. *Science* **1995**, 267, 1629.
- Elghamian, R.; Storhoff, J. J.; Mucic, R. C.; Letsinger, R. L.; Mirkin, C. A. *Science* **1997**, 277, 1078.
- Taton, T. A.; Mirkin, C. A.; Letsinger, R. L. *Science* **2000**, 289, 1757.
- Sandhu, K. K.; McIntosh, C. M.; Simard, J. M.; Smith, S. W.; Rotello, V. M. *Bioconjugate Chem.* **2002**, 13, 3.
- Nikoobakht, B.; Wang, Z. L.; El-Sayed, M. A. *J. Phys. Chem. B* **2000**, 104, 8635.
- Ying, Y. Y.; Chang, S. S.; Lee, C. L.; Wang, C. R. C. *J. Phys. Chem. B* **1997**, 101, 6661.
- Dujardin, E.; Hsin, L. B.; Wang, C. R. C.; Mann, S. *Chem. Commun.* **2001**, 1264.
- Brown, K. R.; Walter, D. G.; Natan, M. J. *Chem. Mater.* **2000**, 12, 306.
- Nicewarner-Peña, S. R.; Freeman, G. P.; Reiss, B. D.; He, L.; Peña, D. J.; Walton, I. D.; Cromer, R.; Keating, C. D.; Natan, M. J. *Science* **2001**, 294, 137.
- Pickering, H. W.; Wagner, C. J. *Electrochem. Soc.* **1967**, 114, 698.
- Tischer, R. P.; Gerischer, H. Z. *Elektrochem.* **1962**, 62, 50.
- Forty, A. J. *Nature* **1979**, 282, 597.
- Li, R.; Sieradzki, K. *Phys. Rev. Lett.* **1992**, 68, 1168.
- Yoon, J.; Chan, M. H. W. *Phys. Rev. Lett.* **1997**, 78, 4801.
- Erlebacher, J.; Aziz, M. J.; Karma, A.; Dimitrov, N.; Sieradzki, K. *Nature* **2001**, 410, 450.
- Williams, D. E.; Newman, R. C.; Song, Q.; Kelly, R. G. *Nature* **1991**, 350, 216.
- Sieradzki, K. *J. Electrochem. Soc.* **1993**, 140, 2868.
- Newman, R. C.; Sieradzki, K. *Science* **1994**, 263, 1708.
- Wagner, K.; Brankovic, S. R.; Dimitrov, N.; Sieradzki, K. *J. Electrochem. Soc.* **1997**, 144, 3545.
- Natarajan, S. R.; Krishnan, K. *Met. Finish.* **1971**, 50, 51.
- Sánchez, H.; Chainet, E.; Nguyen, B.; Ozil, P.; Meas, Y. *J. Electrochem. Soc.* **1996**, 143, 2799.
- Elkington, G.; Elkington, H. British Patent 8847, 1840.
- Winters, E. D. *Plating* **1972**, 59, 213.
- Losi, S. A.; Zuntini, F. L.; Meyer, A. R. *Electrodeposition Surf. Treat.* **1972**, 1, 3.
- Angerer, H.; Ibl, N. *J. Appl. Electrochem.* **1979**, 9, 219.
- Okinaka, Y.; Koch, F. B.; Wolowodiuk, C.; Blessington, D. R. *J. Electrochem. Soc.* **1978**, 125, 1745.
- Koch, F. B.; Okinaka, Y.; Wolowodiuk, C.; Blessington, D. R. *Plating* **1980**, 67, 50.
- Wang, X.; Issaev, N.; Osteryoung, J. G. *J. Electrochem. Soc.* **1998**, 145, 974.
- Chu, W.; Schattenburg, M. L.; Smith, H. I. *Microelectron. Eng.* **1992**, 17, 223.
- Whitney, T. M.; Jiang, J. S.; Searson, P. C.; Chien, C. L. *Science* **1993**, 261, 316.
- Martin, C. R. *Adv. Mater.* **1991**, 3, 457.
- Martin, C. R. *Science* **1994**, 266, 1961.
- Schwanbeck, H.; Schmidt, U. *Electrochim. Acta* **2000**, 45, 4389.
- Baumgärtner, M. E.; Raub, Ch. J. *Platinum Met. Rev.* **1988**, 32, 188.
- Ji, C.; Oskam, G.; Ding, Y.; Erlebacher, J. D.; Wagner, A. J.; Searson, P. C. *J. Electrochem. Soc.*, in press.
- Eisenmann, E. T. *J. Electrochem. Soc.* **1978**, 125, 717.
- Holmbom, G.; Jacobson, B. E.; *J. Electrochem. Soc.* **1988**, 135, 787.
- Chrzanowski, W.; Li, Y. G.; Lasia, A. *J. Appl. Electrochem.* **1996**, 26, 385.
- Zhou, X.; Li, J.; Bodily, D. M.; Wadsworth, M. E. *J. Electrochem. Soc.* **1996**, 140, 1927.
- Cheh, H. Y. *J. Electrochem. Soc.* **1971**, 118, 551.
- MacArthur, D. M. *J. Electrochem. Soc.* **1972**, 119, 672.